Composite Structures 90 (2009) 172–179

Contents lists available at ScienceDirect

Composite Structures

journal homepage: www.elsevier.com/locate/compstruct

Investigating the load transfer efficiency in carbon nanotubes reinforced nanocomposites

Jia-Lin Tsai *, Ting-Chu Lu

Department of Mechanical Engineering, National Chiao Tung University, Hsinchu 300, Taiwan, ROC

ARTICLE INFO

Article history:
Available online 13 March 2009

Keywords:
Nanotubes
Load transfer
Nanocomposites
Shear lag model

ABSTRACT

The load transfer efficiency from surrounding matrix to the carbon nanotubes (CNTs) in the CNTs reinforced nanocomposites was studied. Both single-walled CNTs (SWCNTs) and multi-walled CNTs (MWCNTs) were taken into account in the investigation. A cylindrical representative volume element (RVE) containing the CNTs and matrix phases were employed in the shear lag analysis from which the axial stress distribution as well as the load transfer efficiency in the CNTs was characterized. The effects of the layer number, atomistic interaction of graphite layers, and the aspect ratio of the CNTs on the load transfer efficiency were of concern. Results indicated that the SWCNTs exhibit a greater load transfer efficiency than MWCNTs associated with the same CNTs volume fraction in the nanocomposites. Moreover, the incompetent behaviors of the MWCNTs would become substantial as the number of graphite layers increases, and the deficient load transfer efficiency in the MWCNTs would not be modified effectively even though the chemical bonding between the graphite layers were constructed.

1. Introduction

Because of the exceptional mechanical and physical properties, CNTs have been extensively utilized as reinforcement in nanocomposites materials [1,2]. CNTs are long, hollow cylindrical structures with the length extending from few tens of nanometers to several micrometers and the outer diameters ranging from 2.5 to 30 nm. According to the geometric configuration, the CNTs can be roughly divided into two categories: i.e., one is single-walled CNTs (SWCNTs), and the other is multi-walled CNTs (MWCNTs). The SWCNT is a single graphite sheet that has been rolled into a hollow cylinder. On the other hand, the MWCNTs consist of many concentric graphite layers the interactions of which are dominated by the van der Waals forces.

The load transfer efficiency from the matrix to the CNTs plays an important role in the mechanical response of the CNTs nanocomposites since it may affect the effectiveness of the reinforcements. Haque and Ramasetty [3] utilized the shear lag model to investigate the effects of CNTs aspect ratio, CNTs volume fraction, and matrix modulus on stress transfer in SWCNTs nanocomposites, indicating that no significant increase in CNTs axial stress would occur when the CNT volume fraction increases. In addition, the effect of polymer matrix modulus on axial stress distribution of CNTs is negligible. Zalamea et al. [4] employed the shear transfer model as well as the shear lag model to understand the stress transfer from the outermost layer to the interior layers in the MWCNTs. They pointed out that as the layer number increases, the corresponding efficiency decreases. Shen et al. [5] studied the load transfer between the walls of MWCNTs using molecular dynamic simulation and found that loading the outer wall of MWCNTs does not effectively transfer the load to the inner walls. However, when the chemical bonding between the walls is established, it can significantly improve the load transfer to the inner nanotubes. It is noted that in the above investigations, the loadings were applied on the outermost layers of the MWCNTs, and the corresponding stress in the inner layers was then examined by using either the continuum mechanics [4] or the molecular dynamics simulation [5]. Gao and Li [6] incorporated the atomistic structures of the capped SWCNTs in the molecular structure mechanics [7] and render the Young's modulus of the effective cylindrical solids. Subsequently, the shear stress and the axial stress along the effective solid fiber embedded in the matrix was analyzed using shear-lag analysis. Schadler et al. [8] performed tension and compression tests on the MWCNT composites, indicating that the load transfer to the MWCNTs is higher in compression rather than in tension. Furthermore, the Raman peak position indicates that only the outermost layer is stressed in tension; whereas, all the graphite layers respond in compression. Because only van der Waals forces exist between layers of MWCNTs, it is possible that only the outermost layer is subjected to the load while the inner layers still remain in an almost unloaded condition, and the mechanical performance of the CNTs nanocomposites may be deteriorated accordingly [9]. As a result, in order to fully understand the mechanical performance of

* Corresponding author. Tel.: +886 3 5731608; fax: +886 3 5720634.
E-mail address: jialin@mail.nctu.edu.tw (J.-L. Tsai).

0263-8223/$ - see front matter © 2009 Elsevier Ltd. All rights reserved.
doi:10.1016/j.compstruct.2009.03.004

the CNTs nanocomposites, it is required to visit the load transfer issue from the matrix to the CNTs and further to the inner graphite layers, especially for the nanocomposites with MWCNTs as reinforcement.

In this study, both SWCNTs and MWCNTs reinforced nanocomposites were considered to understand load transfer efficiency from the matrix to the CNTs. By assuming that the CNTs are to be uniformly distributed and perfectly aligned in the matrix, a cylindrical representative volume element (RVE) suitable for the shear lag analysis was proposed. The stress transfer from the matrix to the outermost layer and then to the inner layers of MWCNTs was characterized analytically using the shear lag model, and the corresponding axial stress distribution in each graphite layer of MWCNTs was deduced explicitly. Moreover, the effect of interlayer van der Waals interaction on the stress transfer efficiency in the interior layers of MWCNTs was of concern. Finally, the analytical solutions are validated by the finite element analysis.

2. Shear lag model

2.1. Equivalent continuum solid of CNTs

In order to understand the load transfer efficiency in the CNTs nanocomposites with simplicity, the CNTs are assumed to be uniformly distributed and perfectly aligned within the matrix. Based on the characteristics of geometric periodicity, a unit cell containing a single CNT fiber was selected as a representative volume element (RVE) from which the mechanical properties of the CNTs nanocomposites was determined. In principle, the uniform displacement should be applied on the RVE to satisfy the periodic boundary condition. However, results indicated that the tendency of stress distribution in the reinforcement calculated based on the uniform stress boundary condition is quite close to that of the uniform displacement condition [10]. Therefore, the RVE with uniform stress condition was adopted alternatively for the investigation of the stress distribution in CNTs. In general, MWCNTs and SWCNTs are utilized as reinforcement in the nanocomposites. Without loss of generality, the three-walled CNTs were employed in the following derivation for the determination of the axial stress distribution in each graphite layer and the associated load transfer efficiency as well.

The atomistic configuration of three-walled CNTs is that the diameters of the outermost layer and the innermost layer are D_1 and D_3, respectively, and for the middle layer, it is D_2. To investigate the load transfer efficiency using the continuum mechanics approach, the discrete graphite structures of CNTs has to be transformed into a continuous cylindrical shell as shown in Fig. 1. According to the molecular simulation and experimental observation, it was found that the interlayer spacing "h" of the MWCNTs is around 0.34 nm [11]. As a result, in the construction of equivalent continuum solid of the CNTs, we assumed that the thickness of each equivalent layer is equal to "h" such that the adjacent continuous layers are attached to each other. Through the geometric correlation, the parameter R_{1o}, R_{1i}, R_{2i}, and R_{3i} representing the inner and outer radius of each continuum layer in the equivalent solid can be expressed in terms of the atomistic configuration of CNTs as $R_{1o}=\frac{D_1+h}{2}, R_{1i}=\frac{D_2+h}{2}, R_{2i}=\frac{D_3+h}{2},$ and $R_{3i}=\frac{D_3-h}{2}$.

2.2. Stress distribution in MWCNTs

By means of the shear lag model together with the continuum cylindrical structures of CNTs, the stress distribution in the three-walled CNTs embedded in polymeric nanocomposites was calculated. Fig. 2 demonstrates the RVE employed in the shear lag analysis. It is noted both the axial symmetry with respect to

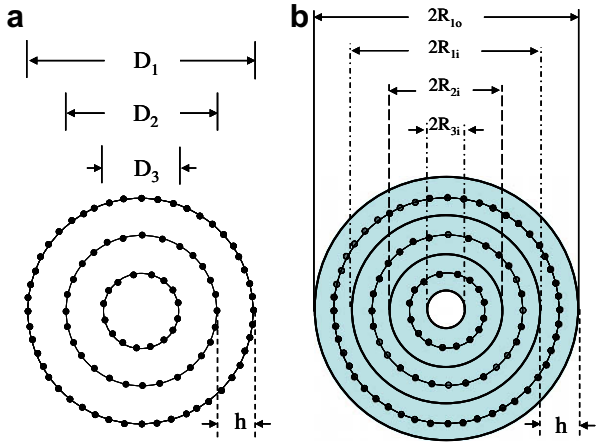

Fig. 1. Conversion of three-walled CNT discrete molecular structure into an equivalent continuum solid ((a) discrete molecular structures, (b) equivalent continuum solid).

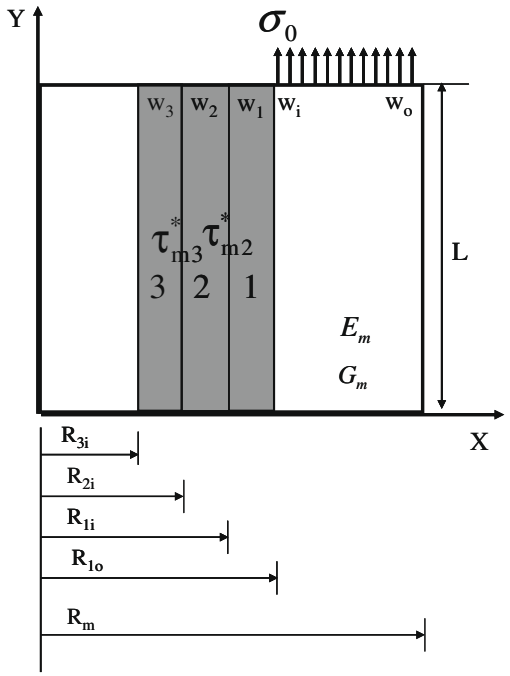

Fig. 2. Schematic of three-walled CNT nanocomposites used in the shear lag analysis.

Y axis and the symmetry to X axis were accounted in the analysis. In Fig. 2, R_{1o} and R_{1i} indicate the outermost layers' outer and inner radii, respectively, and R_{2i} is the inner radius of the second layer, and R_{3i} is the inner radius of the third layer. R_m is the radius of the RVE, and thus the volume fraction of the CNTs is derived as $\frac{R_{1o}^2}{R_m^2}$. In addition, σ_{mo}, τ_{mo}, and w_o, respectively, denote the normal stress, the shear stress, and the vertical deformation of the matrix at the boundary; σ_{mi}, τ_{mi}, and w_i represent the normal stress, shear stress, and normal displacement of the matrix at the interface to layer 1, respectively. w_1, w_2, and w_3 designate the normal displacement of the layers 1, 2, and 3, respectively. Moreover, τ_{mi} is the shear stress on the outermost layer/matrix interface, and τ_{m2}^* and τ_{m3}^* are the shear stress between the layer 1 and layer 2, and layer 2 and layer 3, respectively, as shown in Fig. 2. In generally, the 3-D structure of the nanotubes–resin composites has to be considered in the analysis. In this study, the original 3-D model is simplified as

a cylindrical type structure such that the axial symmetry condition (2D RVE) can be applied for reducing the computing cost. It is noted in performing the simplification process, the volume fraction of the CNTs as well as the material properties remain the same.

From the equilibrium condition in '*Y*' direction, the governing equations for the infinitesimal element of the layer 1 is written as

$$\frac{d\sigma_{f1}}{dy} = -2\frac{R_{1o}\cdot\tau_{mi} - R_{1i}\cdot\tau^*_{m2}}{R^2_{1o} - R^2_{1i}} \tag{1}$$

Similarly, for layers 2 and 3, they were obtained as

$$\frac{d\sigma_{f2}}{dy} = -2\frac{R_{1i}\cdot\tau^*_{m2} - R_{2i}\cdot\tau^*_{m3}}{R^2_{1i} - R^2_{2i}} \tag{2}$$

$$\frac{d\sigma_{f3}}{dy} = -2\frac{R_{2i}\cdot\tau^*_{m3}}{R^2_{2i} - R^2_{3i}} \tag{3}$$

In the classical shear lag model analysis [12], the normal stress variation is considered only in the loading direction ("*Y*" direction) and ignored the transverse direction ("*X*" direction). So, based on the equilibrium equation of the matrix in the *Y* direction, the shear stress distribution in the matrix can be expressed as

$$\tau_m = \frac{\tau_{mi}(b + R_{10} - x)}{b}. \tag{4}$$

It is noted that the relation $b = R_m - R_{10}$ was implemented in the above expression. From the strain and displacement relationship together with the constitutive equation, the shear stress τ_m can be further written in terms of the displacement as

$$\tau_m = G_m\gamma_m = G_m\frac{dw}{dx} \tag{5}$$

where G_m is the shear modulus of the matrix. From Eqs. (4) and (5), the shear stress at the interface between the matrix and the layer 1 is calculated as

$$\tau_{mi} = \frac{2}{b}G_m(w_o - w_i) \tag{6}$$

Substituting Eq. (6) into Eq. (4) leads to

$$\tau_m = \frac{2G_m}{b^2}(b + R_{1o} - x)(w_o - w_i) \tag{7}$$

By combining Eqs. (5) and (7) and then performing integrations on both sides, the displacement field of the matrix w_m is expressed in terms of the displacements at the boundary and interface by

$$w_m = w_i + \frac{1}{b^2}\left[-2bR_{1o} - R^2_{1o} + 2(b + R_{1o})x - x^2\right](w_o - w_i) \tag{8}$$

where w_o and w_i represent the normal displacement of the matrix at the boundary and the interface, respectively. If 1-D elasticity was assumed, the corresponding normal stress in the matrix can be further deduced as

$$\sigma_m = \sigma_{mi} + \frac{1}{b^2}\left[-2bR_{1o} - R^2_{1o} + 2(b + R_{1o})x - x^2\right](\sigma_{mo} - \sigma_{mi}) \tag{9}$$

where $R_{1o} \leqslant x \leq R_m$. The shear stresses ($\tau^*_{m2}$ and τ^*_{m3}) governing the tangential sliding between the adjacent layers was assumed linearly dependent on the difference of the axial displacement of the associated layers as [4]

$$\tau^*_{m2} = G^*_{12}\frac{w_1 - w_2}{h} \tag{10}$$

$$\tau^*_{m3} = G^*_{12}\frac{w_2 - w_3}{h} \tag{11}$$

where $w_1, w_2,$ and w_3 are axial deformations of layers 1, 2, and 3; G^*_{12} is the shear modulus that dominates the degree of the atomistic interaction between the neighboring graphite layers. In fact, the extent of atomistic interaction between the graphite layers should be evaluated through molecular mechanics [11]. However, in the continuum mechanics approach, to effectively demonstrate the influence of the interaction on the load transfer efficiency, the interfacial shear modulus "G^*_{12}" was employed instead to characterize the degree of the interaction.

From the equilibrium condition of the RVE in the *Y* direction,

$$\sigma_0\pi\left[(b + R_{1o})^2 - R^2_{1i}\right] = \sigma_{f1}\pi(R^2_{1o} - R^2_{1i}) + \sigma_{f2}\pi(R^2_{1i} - R^2_{2i}) + \sigma_{f3}\pi(R^2_{2i} - R^2_{3i}) + \int_{R_{1o}}^{R_{1o}+b}\int_0^{2\pi}\sigma_m x d\theta dx \tag{12}$$

together with Eq. (9), the normal stress of the matrix at the boundary is written explicitly as

$$\sigma_{mo} = \sigma_{mi} + \frac{6\left\{\begin{array}{l}\sigma_0\left[(b + R_{1o})^2R^2_{1i}\right] - \sigma_{f1}(R^2_{1o} - R^2_{1i}) - \sigma_{f2}(R^2_{1i} - R^2_{2i})\\ -\sigma_{f3}(R^2_{2i} - R^2_{3i}) - \sigma_{mi}(b^2 + 2bR_{10})\end{array}\right\}}{(8bR_{1o} + 5b^2)} \tag{13}$$

It is noted that the interface bonding between the CNTs outmost layers and matrix was assumed perfect, so the following relation is satisfied

$$\sigma_{mi} = \frac{E_m}{E_f}\sigma_{f1} \tag{14}$$

where E_m and E_f are the Young's moduli of the matrix and the graphite layers, respectively; σ_{mi} is the matrix normal stress at the interface. Substituting Eqs. (6), (10), and (11) into Eqs. (1)–(3) and then taking the derivative with respect to *y* on both sides yields

$$\frac{d^2\sigma_{f1}}{dy^2} = \frac{-2}{R^2_{1o} - R^2_{1i}}\left[\frac{2R_{1o}G_m(\sigma_{mo} - \sigma_{mi})}{bE_m} - \frac{2R_{1i}G^*_{12}(\sigma_{f1} - \sigma_{f2})}{E_f(R_{1o} - R_{2i})}\right] \tag{15}$$

$$\frac{d^2\sigma_{f2}}{dy^2} = \frac{-4G^*_{12}}{(R^2_{1i} - R^2_{2i})E_f}\left[\frac{R_{1i}(\sigma_{f1} - \sigma_{f2})}{R_{1o} - R_{2i}} - \frac{R_{2i}(\sigma_{f2} - \sigma_{f3})}{R_{1i} - R_{3i}}\right] \tag{16}$$

$$\frac{d^2\sigma_{f3}}{dy^2} = \frac{-4R_{2i}G^*_{12}(\sigma_{f2} - \sigma_{f3})}{E_f(R_{1i} - R_{3i})(R^2_{2i} - R^2_{3i})} \tag{17}$$

By combining Eqs. (13)–(17), the axial stress distributions, σ_{f1}, σ_{f2}, and σ_{f3} in the cylindrical layers of the three-walled CNTs was deduced explicitly as

$$\begin{aligned}\frac{d^2\sigma_{f1}}{dy^2} = {} & \left\{\frac{24R_{1o}G_m}{bE_m(R^2_{1o} - R^2_{1i})(8bR_{1o} + 5b^2)}\left[(R^2_{1o} - R^2_{1i}) + \frac{E_m}{E_f}(b^2 + 2bR_{10})\right] + \frac{4R_{1i}G^*_{12}}{E_f(R_{1o} - R_{2i})(R^2_{1o} - R^2_{1i})}\right\}\sigma_{f1}\\ & + \left\{\frac{24R_{1o}G_m(R^2_{1i} - R^2_{2i})}{bE_m(R^2_{1o} - R^2_{1i})(8bR_{1o} + 5b^2)} - \frac{4R_{1i}G^*_{12}}{E_f(R_{1o} - R_{2i})(R^2_{1o} - R^2_{1i})}\right\}\sigma_{f2}\\ & + \left[\frac{24R_{1o}G_m(R^2_{2i} - R^2_{3i})}{bE_m(R^2_{1o} - R^2_{1i})(8bR_{1o} + 5b^2)}\right]\sigma_{f3}\\ & + \frac{-24R_{1o}G_m}{bE_m(R^2_{1o} - R^2_{1i})(8bR_{1o} + 5b^2)}\left[(b + R_{1o})^2 - R^2_{1i}\right]\sigma_0\end{aligned} \tag{18}$$

$$\begin{aligned}\frac{d^2\sigma_{f2}}{dy^2} = {} & \frac{-4R_{1i}G^*_{12}}{E_f(R^2_{1i} - R^2_{2i})(R_{1o} - R_{2i})}\sigma_{f1}\\ & + \frac{4G^*_{12}}{E_f(R^2_{1i} - R^2_{2i})}\left(\frac{R_{1i}}{R_{1o} - R_{2i}} + \frac{R_{2i}}{R_{1i} - R_{3i}}\right)\sigma_{f2}\\ & - \frac{4R_{2i}G^*_{12}}{E_f(R^2_{1i} - R^2_{2i})(R_{1i} - R_{3i})}\sigma_{f3}\end{aligned} \tag{19}$$

$$\frac{d^2\sigma_{f3}}{dy^2} = \frac{-4R_{2i}G^*_{12}}{E_f(R_{1i} - R_{3i})(R^2_{2i} - R^2_{3i})}\sigma_{f2} + \frac{4R_{2i}G^*_{12}}{E_f(R_{1i} - R_{3i})(R^2_{2i} - R^2_{3i})}\sigma_{f3} \tag{20}$$

With the six boundary conditions, σ_{f1}, σ_{f2}, and $\sigma_{f3} = 0$ at $y = L$ and τ_{mi}, τ^*_{m2}, and $\tau^*_{m3} = 0$ at $y = 0$, the system of differential Eqs. (1)–(3), (18), (19), (and) (20) were solved simultaneously using a numerical method from which the axial stress distribution of the graphite layers in the three-walled CNTs were evaluated. In this study, the system of differential equations with boundary value problem were converted into initial value problem by using Newton method and then solved by the Runge–Kutta method [13].

For comparison purposes, the stress distribution of SWCNTs embedded in the matrix was also investigated in the same manner, and the resulting formulation is written as

$$\sigma_f = \frac{\left[(b+R_{1o})^2 - R_{1i}^2\right]\sigma_0}{\left(\left(R_{1o}^2 - R_{1i}^2\right) + \frac{E_m}{E_f}(b^2 + 2bR_{10})\right)} - \frac{e^{\alpha y} + e^{-\alpha y}}{e^{\alpha L} + e^{-\alpha L}} \frac{\left[(b+R_{1o})^2 - R_{1i}^2\right]}{\left((R_{1o}^2 - R_{1i}^2) + \frac{E_m}{E_f}(b^2 + 2bR_{1o})\right)}\sigma_0$$

$$\alpha = \left[\frac{24R_{1o}G_m}{(R_{1o}^2 - R_{1i}^2)(8bR_{1o} + 5b^2)bE_m}\left(\left(R_{1o}^2 - R_{1i}^2\right) + \frac{E_m}{E_f}\left(b^2 + 2bR_{10}\right)\right)\right]^{\frac{1}{2}} \tag{21}$$

where R_{1o} and R_{1i} indicate the outer and inner radii of the SWCNT graphite layer, respectively. By letting the SWCNT length L in Eq. (21) equal to infinity, the saturated stress σ_f^s in the SWCNTs can be determined as

$$\sigma_f^s = \frac{\left[(b+R_{1o})^2 - R_{1i}^2\right]\sigma_0}{\left(\left(R_{1o}^2 - R_{1i}^2\right) + \frac{E_m}{E_f}\left(b^2 + 2bR_{10}\right)\right)} \tag{22}$$

It is noted that in the calculation of stress distribution of the SWCNTs, the outer diameter of the SWCNT is assigned to be the same as that of the outermost layer of the three-walled CNT so that the volume fractions of the reinforcement in the nanocomposites can remain the same.

2.3. Effective length

In order to effectively quantify the load transfer efficiency from the surrounding matrix to the SWCNTs, the concept of effective length of the CNTs is introduced as

$$L_{\text{eff}} = \frac{\int_0^L \sigma_f dy}{\sigma_f^s} \tag{23}$$

where σ_f is the axial stress in the SWCNTs, and σ_f^s is the corresponding saturated stress. In designing nanocomposites materials, the main concept is to facilitate the load applied on the materials being efficiently transferred into the reinforcement and then carried by the reinforcement. Indeed, the effective length can be regarded as an index to evaluate the effectiveness of the reinforcement embedded in the matrix. When the effective length is increasing, it indicates that the load carrying efficiency of the reinforcement is increasing, and thus the overall mechanical properties of the nanocomposites can be enhanced accordingly. The limiting case is that when the effective length of the reinforcement is equal to its full length, the mechanical properties of the composites can be predicted properly using the well-known formula, "rule of mixture". Otherwise, the effective length of the reinforcement has to be accounted for in the modeling of composites properties. When the effective length concept was extended into the three-walled CNTs, the effective length of each layer was calculated and then taken in average as

$$L_{eff} = \frac{\int_0^L (\sigma_{f1} + \sigma_{f2} + \sigma_{f3})dy}{3\sigma_f^s} \tag{24}$$

Table 1
Materials properties of three-walled CNT and matrix adopted in the shear lag model and FEA analysis.

	Graphite layers	Interphase	Matrix
Young's modulus (GPa)	1000		3.0
Poisson's ratio	0.35	0.3	0.3
Shear modulus (GPa)		0.13/0.268/4.2/370	

Table 2
The effective length of three-walled CNTs associated with different aspect ratios and shear properties obtained from shear lag model.

Aspect ratio of CNTs	Shear modulus G_{12}^* (GPa)			
	0.13	0.268	4.2	370
	Effective length of CNTs			
50	0.4496	0.4588	0.4693	0.4725
100	0.5134	0.518	0.5233	0.5263
500	0.5645	0.5654	0.5665	0.5693

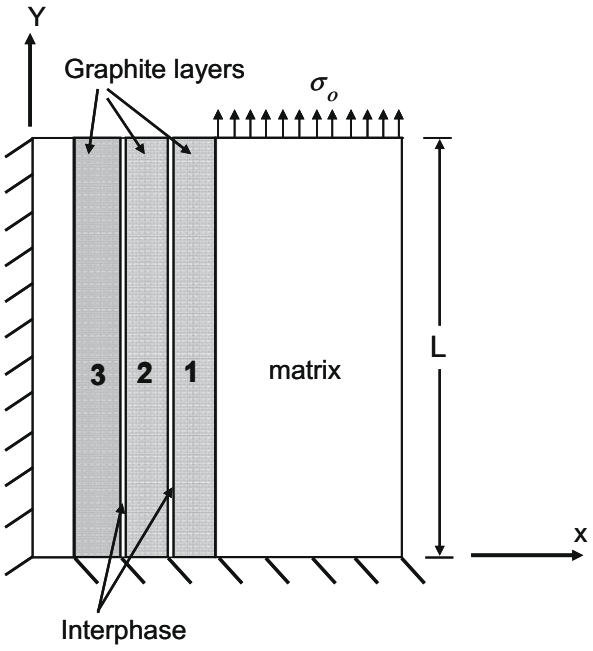

Fig. 3. FEA model for three-walled CNT nanocomposites.

where σ_{f1}, σ_{f2}, and σ_{f3} indicate the axial stress in the layers 1, 2, and 3, respectively, which can be determined from the shear lag analysis addressed in the previous section.

In addition, to understand the atomistic interaction effect of the adjacent graphite layers on the load transfer efficiency of MWCNTs, different values of shear modulus "G_{12}^*", i.e., 0.13, 0.268, 4.2, and 370 GPa, were adopted individually into Eqs. (10) and (11) and then utilized for the calculation of the effective length. It is noted that the first three values obtained from either the molecular mechanics analysis or the experimental measurement were found independently in the literatures [11,14,15], and on the other hand, the value of 370 GPa is calculated according to the postulation that the covalent bond was established in the neighboring graphite layers if possible. The variation of the shear modulus for the graphene sheet constructed by covalent bond is from 384 to 482 GPa [11,16–18], depending on the potential function used to describe the covalent bond. It is noted that the value of 370 GPa was obtained from our molecular dynamics simulation according to the potential function provided in the literature [19]. Although the calculated value is

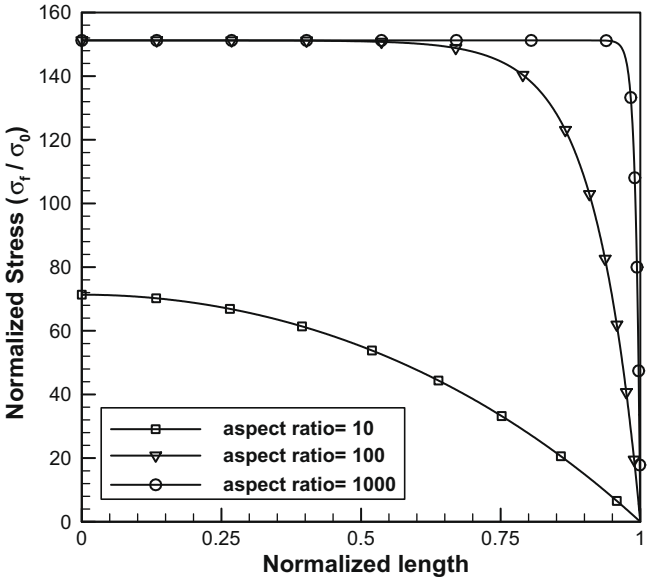

Fig. 4. Stress distribution in the single-walled CNTs.

little different from those in the references, it was adopted to represent the equivalent shear modulus of the covalent bond. The material properties used in the shear lag model and FEM analysis for the three-walled CNT and matrix system are presented in Table 1, and the results of the effective length associated with different shear moduli G_{12}^{*} and aspect ratio are presented in Table 2.

3. Finite element analysis

The load transfer efficiency calculated based on the shear lag model was validated using the finite element analysis (FEA). Because of the cylindrical attribute of the RVE, an axial symmetric FEA model shown in Fig. 3 was employed in the evaluation of the stress distribution on the CNTs nanocomposites. To simulate the extent of interlayer interaction, a thin layer of effective interphase was introduced between the adjacent graphite layers as shown in Fig. 3. The thickness of the effective interphase is selected to be 0.01 nm since results illustrate that when the thickness is much less than the layer thickness "h", it may not have significant effects on the axial stress distributions of the CNTs. For the three-walled CNTs, the geometric parameters, R_{1o} = 1.7 nm, R_{1i} = 1.36 nm, R_{2i} = 1.02 nm, R_{3i} = 0.68 nm, and R_m = 17 nm, were implemented in the FEM

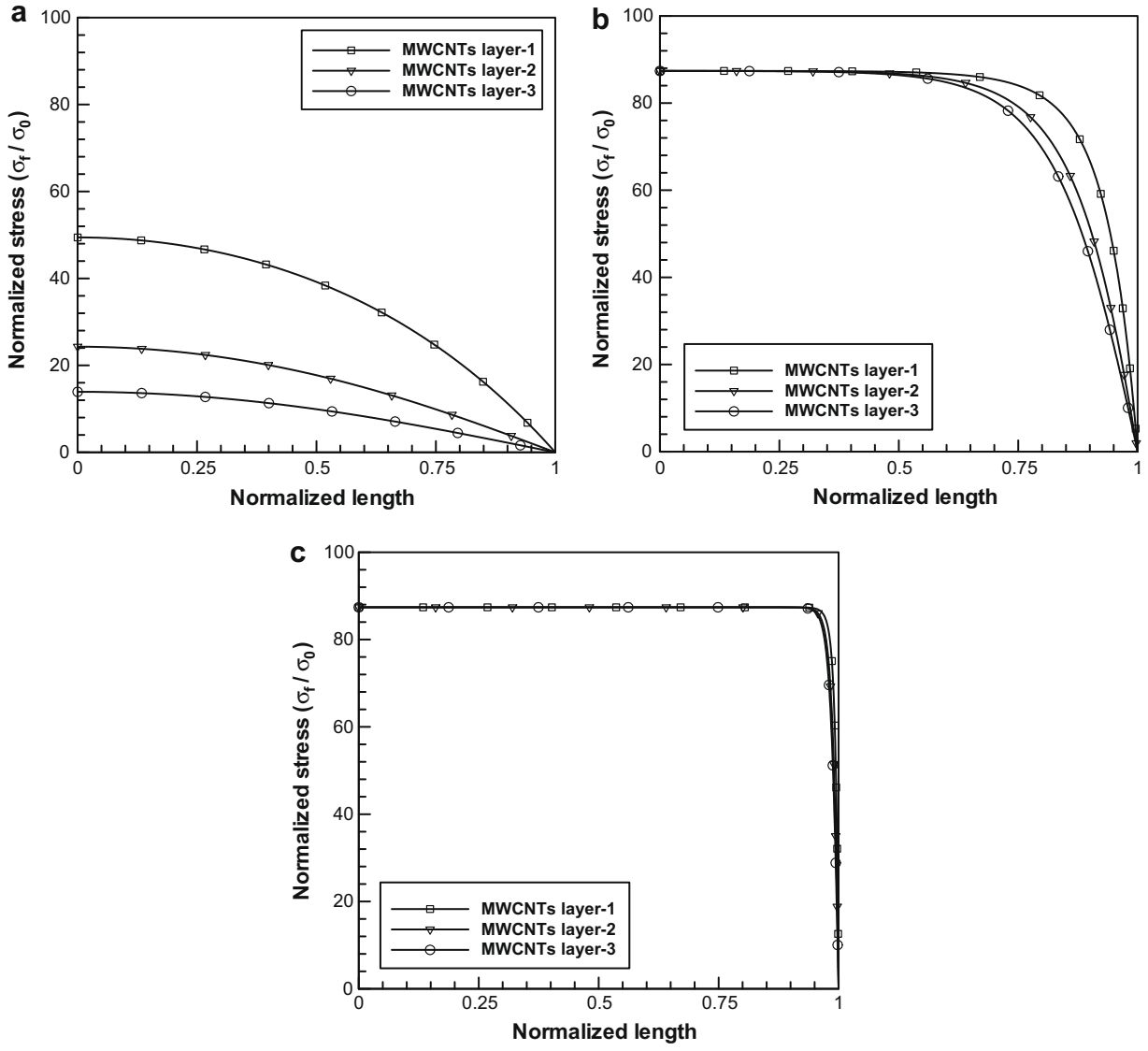

Fig. 5. Stress distribution in the multi-walled CNT (Three-walled CNTs) (a) aspect ratio = 10, (b) aspect ratio = 100, and (c) aspect ratio = 1000. ($G^{*} = 0.268$).

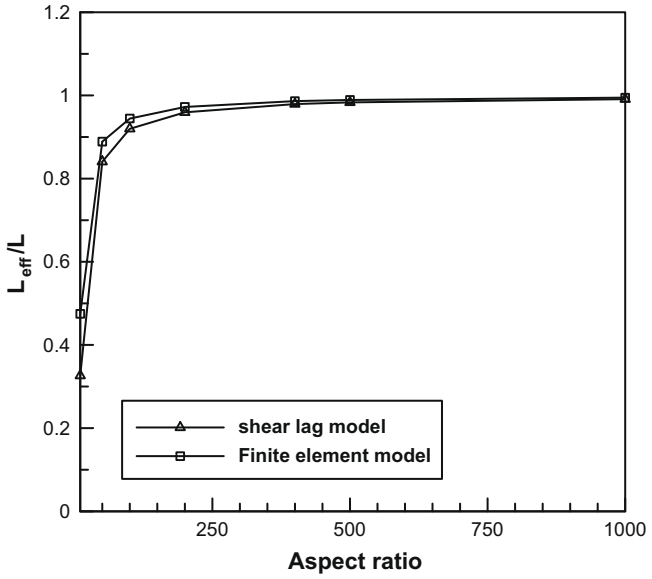

Fig. 6. Comparison of the load transfer efficiency obtained from shear-lag model and FEA analysis (single-walled CNTs case).

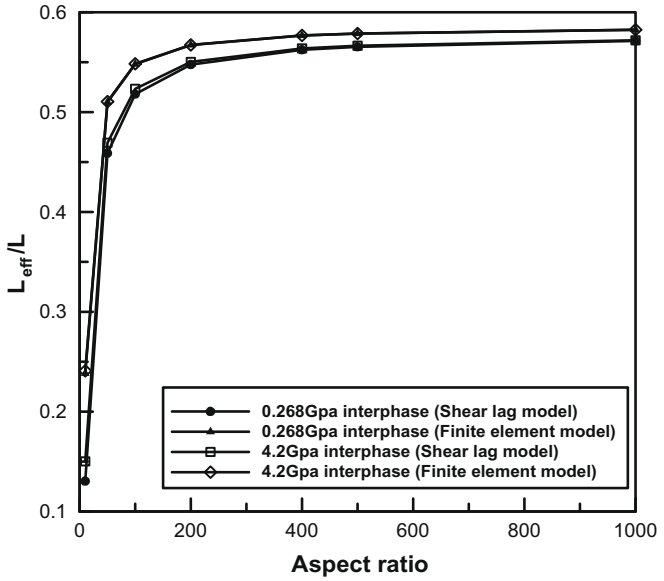

Fig. 7. Comparison of the load transfer efficiency obtained form shear-lag model and FEA (three-walled CNTs case).

Table 3
Comparison of the effective lengths of single-walled CNTs calculated based on shear lag model and finite element model.

Aspect ratio of CNTs	L_{eff}/L		
	Shear lag model	Finite element model	Difference (%)
10	0.3220	0.4748	47.45
50	0.8395	0.8889	5.88
100	0.9193	0.9445	2.74
200	0.9591	0.9724	1.39
400	0.9791	0.9863	0.74
500	0.9830	0.9891	0.62
1000	0.9910	0.9947	0.37

analysis. It should be noted that the effective interphase somewhere in between the graphite layers was shared by the neighboring layers such that the "true" thickness of graphite layers 1 and 3 becomes 0.335 nm, and layer 2 is 0.33 nm. Again, different values of shear modulus were also considered in the effective interphase to simulate the atomistic interaction of the graphite layers, and the results were compared with the shear lag predictions.

4. Results and discussions

The axial stress distributions for the single-walled CNTs obtained from shear lag analysis in terms of different aspect ratios are shown in Fig. 4. It seems that when the aspect ratio of the CNTs is low, the axial stress may not be able to attain the saturated point. In addition, the axial stress distributions of the three-walled CNTs obtained from shear lag analysis associated with different aspect ratios are illustrated in Fig. 5 where the shear modulus G_{12}^{*} is 0.268 GPa. It can be seen that in all three layers, the stresses increase from the CNTs ends and gradually attains the saturated value. Moreover, in the outermost layer, the stress is relatively higher and the saturation rate is also faster than that in the inner layers. Apparently, the outermost layer demonstrates better load transfer efficiency than the inner layers. It should be mentioned that if the aspect ratio of the CNTs is not high enough, the saturated stress may not be accomplished in the CNTs as shown in Fig. 5a. In addition, it was found that the saturated stress in the three-walled CNT is still less than that in the SWCNTs calculated from Eq. (22) even though the MWCNTs aspect ratio is up to 1000. The effective lengths of the SWCNT associated with different aspect ratios obtained from shear lag model and FEM analysis are compared in Fig. 6. The percentage difference between the two approaches is listed in Table 3. It is shown that when the aspect ratio of the SWCNT is less than 100, the effective length predicted by FEM analysis are little higher than that obtained from the shear lag model. However, as the aspect ratio of the CNTs is more than 100, the discrepancy between the two predictions becomes unsubstantial. When the aspect ratio of the CNTs increase, the effective length increases accordingly, and the ratio of effective length to the CNT length almost reach to 1 as the aspect ratio is up to 1000. Thus, exhibiting the superior load transfer efficiency, the SWCNT with higher aspect ratio make it possible to become a good

Table 4
Comparison of the effective lengths of multi-walled CNTs calculated based on shear lag model and finite element model.

Aspect ratio of CNTs	L_{eff}/L ($G_{12}^{*} = 0.268$ GPa)			L_{eff}/L ($G_{12}^{*} = 4.2$ GPa)		
	Shear lag model	Finite element model	Difference (%)	Shear lag model	Finite element model	Difference (%)
10	0.1304	0.2384	82.82	0.1502	0.2409	60.39
50	0.4588	0.5100	11.16	0.4693	0.5105	8.78
100	0.5180	0.5481	5.81	0.5233	0.5484	4.80
200	0.5476	0.5672	3.58	0.5503	0.5673	3.09
400	0.5624	0.5768	2.56	0.5638	0.5768	2.31
500	0.5654	0.5787	2.35	0.5665	0.5787	2.15
1000	0.5713	0.5825	1.96	0.5719	0.5825	1.85

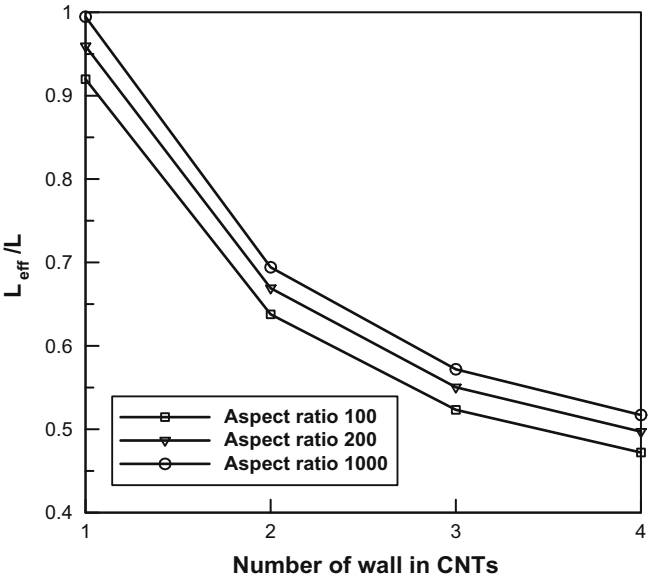

Fig. 8. The effect of number of CNTs layers and aspect ratio on load transfer efficiency (based on shear lag model).

reinforcement in the nanocomposites. On the other hand, for the multi-walled CNTs, e.g., three-walled CNT as shown in Fig. 7, even though the aspect ratio is up to 1000, the ratio of the effective length with respect to the total length is still around 0.55. This phenomenon clearly illustrates the fact that because the lower saturated stress induced in the multi-walled CNTs, the load transfer efficiency in the MWCNT is not as good as compared to SWCNTs. Furthermore, the interphase shear modulus play a minor role in the load transfer efficiency of MWCNTs since no significant differences in the effective length were observed in the two cases, i.e., $G^* = 4.2$ GPa and $G^* = 0.268$ GPa. A comparison of the FEM results with shear lag model for the MWCNTs indicates that there still is distinction in the effective length predictions although the trends for the effective length in terms of aspect ratio are basically the same. This difference could be due to the different treatments of the interactions in the neighboring graphite layers. In the shear lag model, the associated interaction is modeled by the tangential sliding between the neighboring layers in terms of a linear shear stiffness relationship [4]. On the contrary, in the FEM model, the interaction is characterized by the introduction of an interphase with shear properties. The percentage difference between the FEM model and shear lag model for the three-walled CNTs is presented in Table 4. Fig. 8 plots the effective length versus the number of the graphite layers in MWCNTs. It is indicated that as the layer number increases, the ineffective attribute in the multi-wall CNT become more appreciable. The poor load transfer efficiency in MWCNTs could be responsible for the reduction of the stiffness of the nanocomposites. On the other hand, the wavy CNTs may also influence the load transfer efficiency as well as the stiffness of the nanocomposites, which was not taken into account in the analysis. In light of the forgoing discussions regarding the load transfer efficiency of the MWCNTs, it was suggested that the MWCNTs may not play a good role as being reinforcement in the nanocomposites. It is noted that in the above comparison, the volume fractions of MWCNTs and SWCNTs in the nanocomposites are kept the same and equal to 1%.

In an attempt to improve the load transfer efficiency of MWCNTs, the chemical bonding between the graphite layers could be established through chemical modification [20,21]. To simulate the contribution of chemical bonding on the load transfer efficiency in the MWCNT nanocomposites, the shear modulus between inter-atomistic graphite layers was postulated as 370 GPa (the shear modulus of graphite sheet). In addition, for the sake of comparison, the associated shear modulus varying from 0.13, 0.268, to 4.2 GPa were also implemented in the analysis to simulate van der Waals interaction, and the results corresponding to different aspect ratio of MWCNTs are all presented in Table 2. Results depicted that even though the shear modulus is up to 370 GPa, the load transfer efficiency in MWCNTs is not improved dramatically as compared to the other cases with lower shear modulus. When the covalent bond was established between the graphite layers, MD simulation revealed that the load transfer from the outer layer to the inner layers can be enhanced accordingly [5]. Nonetheless, even though the load carrying capacity in the inner layers is improved, the amount of load carried by the inner layers is still much less than that in the outermost layer. As a result, for the MWCNTs, the overall improvement in terms of load transfer efficiency caused by the chemical bond is not considerable. It is suggested that the generation of the chemical bonding between the graphite layers may not be an effective way to enhance the load transfer efficiency in the MWCNTs nanocomposites.

5. Conclusions

The load transfer efficiency in the CNTs reinforced nanocomposites was investigated using the conventional shear lag model and the FEA analysis. The effects of the layer number, inter-graphic layers interaction, and aspect ratio of the CNTs on the load transfer efficiency were examined. It was revealed that basically the load transfer efficiency increases with the increment of the aspect ratio of CNTs. However, as the graphite layer number in MWCNT increase, the load transfer efficiency from the matrix to the MWCNTs is decreasing. Moreover, the inefficient tendency in the MWCNT can not be recovered even if the van der Waals interaction between the adjacent graphic layers is replaced by the chemical bonding. The above observations on the load transfer efficiency in the CNTs nanocomposites based on the shear lag model were all in good agreements with the FEM predictions.

References

[1] Thostenson ET, Li C, Chou TW. Nanocomposites in context. Compos Sci Technol 2005;65(3–4):491–516.
[2] Dresselhaus MS, Dresselhaus G, Avouris PH. Carbon nanotubes synthesis, structure, properties and applications. Berlin: Springer; 2000.
[3] Haque A, Ramasetty A. Theoretical study of stress transfer in carbon nanotube reinforced polymer matrix composites. Compos Struct 2005;71(1):68–77.
[4] Zalamea L, Kim H, Pipes RB. Stress transfer in multi-walled carbon nanotubes. Compos Sci Technol 2007;67:3425–33.
[5] Shen GA, Namilae S, Chandra N. Load transfer issues in the tensile and compressive behavior of multiwall carbon nanotubes. Mater Sci Eng A 2006;429:66–73.
[6] Gao XL, Li K. A shear-lag model for carbon nanotube-reinforced polymer composites. Int J Solids Struct 2005;42:1649–67.
[7] Li C, Chou TW. A structural mechanics approach for the analysis of carbon nanotubes. Int J Solids Struct 2003;40:2487–99.
[8] Schadler LS, Giannaris SC, Ajayan PM. Load transfer in carbon nanotube epoxy composites. Appl Phys Lett 1998;73(26):3842–4.
[9] Lau KT, Gu C, Hui D. A critical review on nanotube and nanotube/nanoclay related polymer composite materials. Compos Part B 2006;37(6):425–36.
[10] Tsai JL, Sun CT. Effect of platelet dispersion on the load transfer efficiency in nanoclay composites. J Compos Mater 2004;38(7):567–79.
[11] Cho J, Luo JJ, Daniel IM. Mechanical characterization of graphite/epoxy nanocomposites by multi-scale analysis. Compos Sci Technol 2007;67:2399–407.
[12] Cox HL. The elasticity and strength of paper and other fibrous materials. Brit J Appl Phys 1952;3:72–9.
[13] Alkis Constantinides. Applied numerical methods with personal computers. New York: McGraw-Hill, Inc.; 1987.
[14] Jenkins GM, Jouquet G. The effect of short-term neutron irradiation on the shear compliance of hot-worked pyrolytic graphite. Carbon 1968;6:85–91.
[15] Dolling G, Brockhouse BN. Lattice vibrations in pyrolitic graphite. Phys Rev 1962;128(3):1120–3.

[16] Xiao JR, Gama BA, Gillespie Jr JW. An analytical molecular structural mechanics model for the mechanical properties of carbon nanotube. Int J Solids Struct 2005;42:3075–92.
[17] Reddy CD, Rajendran S, Liew KM. Equilibrium configuration and continuum elastic properties of finite sized graphene. Nanotechnology 2006;17:864–70.
[18] Blakslee OL, Proctor DG, Seldin EJ, Spence GB, Weng T. Elastic constant of compression annealed pyrolytic graphite. J Appl Phys 1970;41:3373–82.
[19] Li C, Chou TW. Elastic moduli of carbon nanotubes and the effect of van der Waals forces. Compos Sci Technol 2003;63:1517–24.
[20] Banhart F. Irradiation effects in carbon nanostructures. Rep Prog Phys 1999;62(8):1181–221.
[21] Krasheninnikov AV, Nordlund K. Irradiation effects in carbon nanotubes. Nucl Instrum Meth Phys Res B 2004;216:355–66.